

Localization of electromagnetic energy using a left-handed-medium slab

Tie Jun Cui,^{1,*} Qiang Cheng,¹ Wei Bing Lu,¹ Qin Jiang,¹ and Jin Au Kong^{2,3}

¹*Center for Computational Electromagnetics and the State Key Laboratory of Millimeter Waves, Department of Radio Engineering, Southeast University, Nanjing 210096, People's Republic of China*

²*Electromagnetics Academy at Zhejiang University, Zhejiang University, Yu-Quan, Hangzhou 310027, People's Republic of China*

³*Department of Electrical Engineering and Computer Science, Massachusetts Institute of Technology, Cambridge, Massachusetts 02139, USA*

(Received 2 July 2004; revised manuscript received 5 November 2004; published 19 January 2005)

It is well known that a left-handed-medium (LHM) slab with negative permittivity $-\epsilon_0$ and negative permeability $-\mu_0$ in the free space can be made as a perfect lens [J. B. Pendry, Phys. Rev. Lett. **85**, 3966 (2000)], which produces a perfect image of the excitation current source at the perfect-imaging point. In this paper, we first show that such a lossless LHM slab can localize the electromagnetic energy completely through an exact analysis. When two linear sources with opposite current directions are placed at the perfect-imaging points of the LHM slab, we have demonstrated that all electromagnetic waves are confined in a region between the two sources and there is no power radiating outwards the region. In such a region, the propagating modes behave like standing waves, and the field patterns can be controlled by changing the source positions. The evanescent waves which behave like strong plasma surface waves, however, tend to infinity. In practical cases, the perfect lens does not exist and there is usually a mismatch where both the relative permittivity and permeability are different from -1 . In the second part of the paper, the mismatch effect has been considered on the energy localization. We have shown that strong surface waves exist along the two surfaces of the slab, and both the propagating and evanescent waves are nearly confined within the region between the two sources under the mismatch. Such localizations of electromagnetic waves and energies may find important applications in microwave and optical devices.

DOI: 10.1103/PhysRevB.71.045114

PACS number(s): 78.20.Ci, 41.20.Jb, 42.25.Bs, 63.20.Pw

I. INTRODUCTION

In 1968, Veselago introduced the concept of left-handed material (LHM) with simultaneously negative permittivity and negative permeability,¹ which exhibits a lot of unusual properties different from the normal right-handed material (RHM), such as negative refraction index, reversed Doppler shift, and backward Cerenkov radiation. However, such a LHM does not exist naturally and, hence, it has not received much attention until recently. When the artificial LHM was realized using periodic structures since 1996,²⁻⁶ intensive study of LHM has been conducted in the theory, experiments, and potential applications.⁷⁻¹⁴

As predicted by Veselago, a LHM slab could refocus the electromagnetic waves from a point source.¹ Later, Pendry extended Veselago's idea and further predicted that evanescent waves could be amplified through the LHM slab, and the source information can be reconstructed in the perfect imaging point without the loss of amplitude¹⁵ if the permittivity is $-\epsilon_0$ and the permeability is $-\mu_0$. It is well known that evanescent waves carry subwavelength information of an object, hence, the LHM slab could break the Rayleigh diffraction limit of conventional imaging systems. As a consequence, a flat LHM slab with negative permittivity $-\epsilon_0$ and negative permeability $-\mu_0$ can be made as a perfect lens to achieve super-resolution. The perfect lens has been numerically verified in Ref. 16. However, the artificial LHM is always lossy, and the lossy effect on the perfect image has been studied in Refs. 17-21.

The perfect lens produces a perfect image of the excitation current source at the perfect-imaging point. If another

current source with the same amplitude and opposite current direction is placed at the perfect-imaging point, we have shown that in this paper electromagnetic waves are confined completely in a region between the two sources and the electromagnetic fields outside the region are zero. Hence, the LHM slab can be used to localize electromagnetic or optical waves in another way besides the light localization due to structural defects introduced to the regular structure of the photonic crystals²² and the microwave localization using a three-dimensional fractal cavity, the Menger sponge.²³ Actually, the localization of electromagnetic waves could find applications in a variety of optical and microwave devices due to the high quality factor of the localized modes, such as in narrow-band filters and low-threshold lasers.²⁴

However, it is rather difficult to realize a perfect lens because of the mismatch of the relative permittivity and permeability from -1 and the lossy effect. Hence, in the second part of the paper, we will study the localization of electromagnetic waves using a mismatched perfect lens. When two current sources with opposite directions are placed at the perfect imaging points of the slab symmetrically, we show that strong surface waves exist along the two surfaces of the slab, and both the propagating and evanescent waves are nearly confined within the region between the two sources under the mismatch. Numerical experiments validate the above conclusions.

II. LOCALIZATION OF ELECTROMAGNETIC ENERGY USING A PERFECT LENS

Let us consider a general case when a linear source I_1 is located before a perfect lens with negative permittivity $-\epsilon_0$

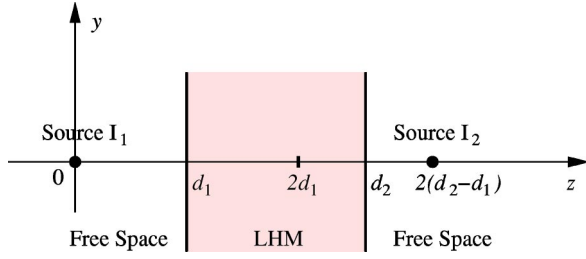


FIG. 1. Two linear currents [two-dimensional (2D) point sources] located at the perfect-imaging points of a LHM slab with negative permittivity $-\epsilon_0$ and negative permeability $-\mu_0$. The two currents have opposite directions.

and negative permeability $-\mu_0$. Suppose that the LHM slab has a thickness of $d=d_2-d_1$, and the linear source is separated from the left side of slab at a distance of d_1 . Under the coordinate system shown in Fig. 1 where the source is positioned at the origin, there will be perfect images at the locations of $z=2d_1$ and $z=2(d_2-d_1)$.¹⁵ From the exact electromagnetic analysis, the electric fields in different regions can be generally written as

$$E_x^{(1)} = -\frac{\omega\mu_0}{4\pi}I_1 \int_{-k_0}^{k_0} \frac{1}{k_{0z}} \tilde{E}_{xp}^{(1)} e^{ik_y y} dk_y - \frac{\omega\mu_0}{4\pi}I_1 \int_{|k_y|>k_0} \frac{1}{i\alpha_{0z}} \tilde{E}_{xe}^{(1)} e^{ik_y y} dk_y, \quad (1)$$

where the first integral corresponds to the propagating waves, the second integral corresponding to the evanescent waves, $k_0 = \omega\sqrt{\mu_0\epsilon_0}$ is the wave number in free space, and

$$k_{0z} = \sqrt{k_0^2 - k_y^2}, \quad \alpha_{0z} = \sqrt{k_y^2 - k_0^2},$$

which are even functions of k_y . In Eq. (1), $\tilde{E}_{xp}^{(1)}$ is the propagating waves in the spectral domain

$$\tilde{E}_{xp}^{(1)} = \begin{cases} e^{-ik_{0z}z}, & z < 0 \\ e^{ik_{0z}z}, & 0 \leq z < d_1 \\ e^{ik_{0z}(2d_1-z)}, & d_1 \leq z < d_2 \\ e^{ik_{0z}[z-2(d_2-d_1)]}, & z \geq d_2, \end{cases} \quad (2)$$

while $\tilde{E}_{xe}^{(1)}$ is the evanescent waves in the spectral domain

$$\tilde{E}_{xe}^{(1)} = \begin{cases} e^{\alpha_{0z}z}, & z < 0 \\ e^{-\alpha_{0z}z}, & 0 \leq z < d_1 \\ e^{-\alpha_{0z}(2d_1-z)}, & d_1 \leq z < d_2 \\ e^{-\alpha_{0z}[z-2(d_2-d_1)]}, & z \geq d_2. \end{cases} \quad (3)$$

If there is another linear source I_2 which is located at the perfect-imaging point $z=2(d_2-d_1)$, we easily obtain the electric fields in different regions as

$$E_x^{(2)} = -\frac{\omega\mu_0}{4\pi}I_2 \int_{-k_0}^{k_0} \frac{1}{k_{0z}} \tilde{E}_{xp}^{(2)} e^{ik_y y} dk_y - \frac{\omega\mu_0}{4\pi}I_2 \int_{|k_y|>k_0} \frac{1}{i\alpha_{0z}} \tilde{E}_{xe}^{(2)} e^{ik_y y} dk_y, \quad (4)$$

where $\tilde{E}_{xp}^{(2)}$ corresponds to propagating waves in the spectral domain

$$\tilde{E}_{xp}^{(2)} = \begin{cases} e^{-ik_{0z}z}, & z < d_1 \\ e^{-ik_{0z}(2d_1-z)}, & d_1 \leq z < d_2 \\ e^{-ik_{0z}[z-2(d_2-d_1)]}, & d_2 \leq z < 2(d_2-d_1) \\ e^{ik_{0z}[z-2(d_2-d_1)]}, & z \geq 2(d_2-d_1), \end{cases} \quad (5)$$

and $\tilde{E}_{xe}^{(2)}$ corresponds to evanescent waves in the spectral domain

$$\tilde{E}_{xe}^{(2)} = \begin{cases} e^{\alpha_{0z}z}, & z < d_1 \\ e^{\alpha_{0z}(2d_1-z)}, & d_1 \leq z < d_2 \\ e^{\alpha_{0z}[z-2(d_2-d_1)]}, & d_2 \leq z < 2(d_2-d_1) \\ e^{-\alpha_{0z}[z-2(d_2-d_1)]}, & z \geq 2(d_2-d_1). \end{cases} \quad (6)$$

Now we consider a special case when $I_1 = -I_2 = I_0$. Based on the addition theorem, the total electric field produced by I_1 and I_2 can be easily determined by the summation of Eqs. (1) and (4). For propagating waves, we have

$$E_{xp}(y, z) = -\frac{i\omega\mu_0}{\pi}I_0 \int_0^{k_0} \frac{1}{k_{0z}} \tilde{E}_{xp} \cos(k_y y) dk_y, \quad (7)$$

where

$$\tilde{E}_{xp} = \begin{cases} \sin k_{0z}z, & 0 \leq z < d_1 \\ \sin k_{0z}(2d_1-z), & d_1 \leq z < d_2 \\ \sin k_{0z}(z-2d_2+2d_1), & d_2 \leq z < 2(d_2-d_1) \\ 0, & \text{elsewhere.} \end{cases} \quad (8)$$

For evanescent waves, we have

$$E_{xe}(y, z) = -\frac{i\omega\mu_0}{\pi}I_0 \int_{|k_y|>k_0} \frac{1}{\alpha_{0z}} \tilde{E}_{xe} \cos(k_y y) dk_y, \quad (9)$$

in which

$$\tilde{E}_{xe} = \begin{cases} \text{sh } \alpha_{0z}z, & 0 \leq z < d_1 \\ \text{sh } \alpha_{0z}(2d_1-z), & d_1 \leq z < d_2 \\ \text{sh } \alpha_{0z}(z-2d_2+2d_1), & d_2 \leq z < 2(d_2-d_1) \\ 0, & \text{elsewhere.} \end{cases} \quad (10)$$

From above formulations, we clearly see that: (1) all electric fields are confined in a region between the two sources; (2) the propagating waves behave like standing waves; (3) the evanescent waves behave like plasma surface waves; (4) the electric field is continuous in all positions along the z axis; and (5) all electric fields are always imaginary.

Using the Maxwell's equation, we know that the magnetic field has both z and y components. For propagating waves, they are written as

$$H_{zp}(y,z) = -\frac{I_0}{\pi} \int_0^{k_0} \frac{k_y}{k_{0z}} \tilde{H}_{zp} \sin(k_y y) dk_y, \quad (11)$$

$$H_{yp}(y,z) = -\frac{I_0}{\pi} \int_0^{k_0} \tilde{H}_{yp} \cos(k_y y) dk_y, \quad (12)$$

where \tilde{H}_{zp} has the same expressions as \tilde{E}_{xp} in most regions except that $\tilde{H}_{zp} = -\sin k_{0z}(2d_1 - z)$ when $d_1 \leq z < d_2$, and

$$\tilde{H}_{yp} = \begin{cases} \cos k_{0z} z, & 0 \leq z < d_1 \\ \cos k_{0z}(2d_1 - z), & d_1 \leq z < d_2 \\ \cos k_{0z}(z - 2d_2 + 2d_1), & d_2 \leq z < 2(d_2 - d_1) \\ 0, & \text{elsewhere.} \end{cases} \quad (13)$$

For evanescent waves, they are written as

$$H_{ze}(y,z) = -\frac{I_0}{\pi} \int_{|k_y| > k_0} \frac{k_y}{\alpha_{0z}} \tilde{H}_{ze} \sin(k_y y) dk_y, \quad (14)$$

$$H_{ye}(y,z) = -\frac{I_0}{\pi} \int_{|k_y| > k_0} \tilde{H}_{ye} \cos(k_y y) dk_y, \quad (15)$$

where \tilde{H}_{ze} has the same expressions as \tilde{E}_{xe} in most regions except that $\tilde{H}_{ze} = -\text{sh } \alpha_{0z}(2d_1 - z)$ when $d_1 \leq z < d_2$, and

$$\tilde{H}_{ye} = \begin{cases} \text{ch } \alpha_{0z} z, & 0 \leq z < d_1 \\ \text{ch } \alpha_{0z}(2d_1 - z), & d_1 \leq z < d_2 \\ \text{ch } \alpha_{0z}(z - 2d_2 + 2d_1), & d_2 \leq z < 2(d_2 - d_1) \\ 0, & \text{elsewhere.} \end{cases} \quad (16)$$

Similar to the electric field, we observe that: (1) all magnetic fields are confined in the region between the two sources; (2) the propagating waves behave like standing waves; (3) the evanescent waves behave like plasma surface waves; (4) the normal components of magnetic fields H_z are discontinuous at the slab boundary $z=d_1$ and $z=d_2$ but B_z are continuous which satisfies the boundary condition; (5) the tangential components of magnetic fields H_y are discontinuous at $z=0$ and $z=2(d_2-d_1)$ due to the existence of linear sources; and (6) the magnetic fields are always real.

Because the electric fields are always imaginary and the magnetic fields are always real, the complex Poynting vectors defined by $\mathbf{S} = \frac{1}{2} \mathbf{E} \times \mathbf{H}^*$ are always imaginary. Hence, the time-averaged power density $\text{Re}(\mathbf{S})$ is always zero, which implies that there is no power radiating outside and no power transmitting inside. All electromagnetic energies are stored within the region between the two sources. The factor $\text{Im}(\mathbf{S})$ is a measure of difference of the electric and magnetic energies.

Physically speaking, when the RHM background and the LHM slab are exactly matched, the field radiated by the source $-I$ goes through the LHM slab, and experiences "time reversed" at the origin which forms a perfect image. In the left region of the source I , the field radiated by the current I

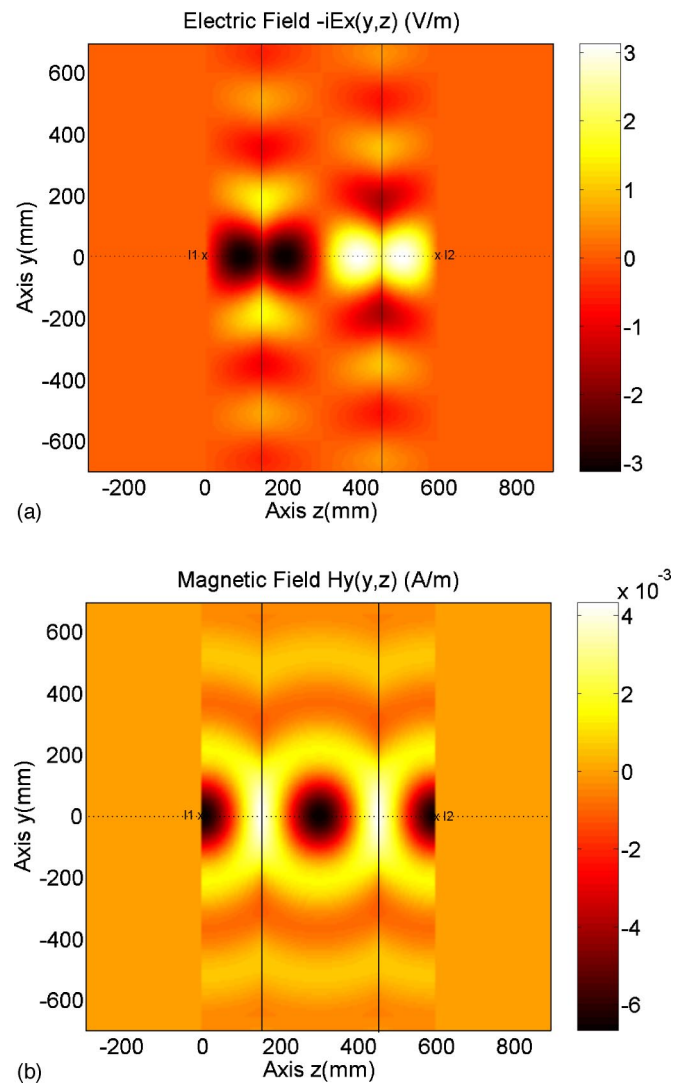


FIG. 2. (Color online) The field patterns of propagating waves within and outside the LHM slab when the frequency is 1 GHz and $d_1=150$ mm and $d_2=450$ mm. (a) Electric field E_{xp} . (b) Magnetic field H_{yp} .

has the same amplitude but opposite direction as that by the source $-I$. Such two fields cancel each other, and the total field in this region is zero. So is it in the right region of the source $-I$.

In order to observe the field distributions between the two sources, we have computed the propagating-wave patterns for a LHM slab when $d_1=150$ mm and $d_2=450$ mm. At the frequency of 1 GHz, the electric and magnetic field patterns are illustrated in Fig. 2 when the source $I_1=1$ mA is located at $z=0$ and the source $I_2=-1$ mA is located at $z=600$ mm. Apparently, both electric and magnetic fields are confined between the two sources and no power radiating outside the region. From Fig. 2, we clearly see that the field patterns behave like standing waves. Both the electric and magnetic fields are symmetrical along the axis $y=0$. With respect to another axis $z=300$ mm, the electric field is anti-symmetrical and the magnetic field is symmetrical.

For evanescent waves, they tend to infinity due to the divergence of the integration. However, we can plot the eva-

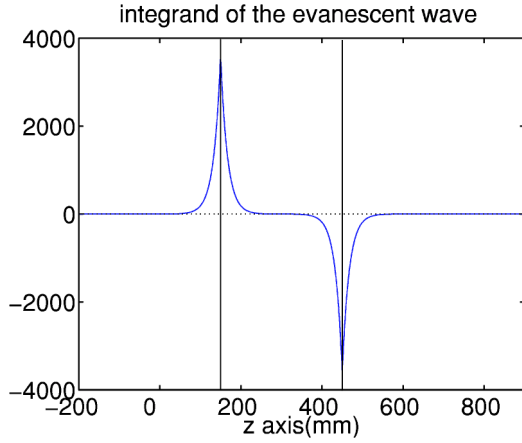


FIG. 3. The evanescent fields \tilde{E}_{xe} in the spectral domain when the frequency is 1 GHz and $d_1=150$ mm, $d_2=450$ mm, $k_y=3k_0$, and $y=0$.

nescent fields in the spectral domain. When $k_y=3k_0$ and $y=0$, the evanescent electric field \tilde{E}_{xe} is shown in Fig. 3, where we clearly observe strong plasma surface waves on two sides of the LHM slab. Also, \tilde{E}_{xe} is continuous along z axis.

We can change the field patterns by moving the source positions. When $d_1=0$ and $d_2=300$ mm, i.e., the source I_1 is located at the left edge of the slab and the source I_2 is located at $z=600$ mm, the electric and magnetic field distributions of propagating waves are illustrated in Fig. 4. In such a case, both the electric and magnetic fields are symmetrical along the axes $y=0$ and $z=300$ mm. Generally, we can control the field patterns for a given LHM slab by changing the source positions.

In above examples, the thickness of LHM slab is only one wavelength. If the frequency increases to 10 GHz, the same LHM slab has a thickness of ten wavelengths. In such a case, the electric and magnetic field patterns of propagating waves are depicted in Figs. 5 and 6 when the sources have different positions. From these figures, we clearly see that the symmetrical property of the patterns is completely the same as that in Figs. 2 and 4. However, more cycles of standing waves are observed at the high frequency.

III. MISMATCH EFFECT OF THE PERFECT LENS ON THE ENERGY LOCALIZATION

In practical cases, however, the perfect lens is hardly realized and there is always a mismatch or loss. In this section, we will study the mismatch effect of the perfect lens on the energy localization. Without losing generality, we consider the case that $\mu_{r2}=-1+\delta$ and $\epsilon_{r2}=-1/(1+\delta)$ to keep the wave numbers in different regions as a constant.²⁵ Here, δ is a real parameter.

For the evanescent waves where k_z is a pure imaginary, $k_z=i\gamma$, the transmission coefficient T of waves propagating from the left region to the right region shown in Fig. 1 can be written in a simple form when δ is small

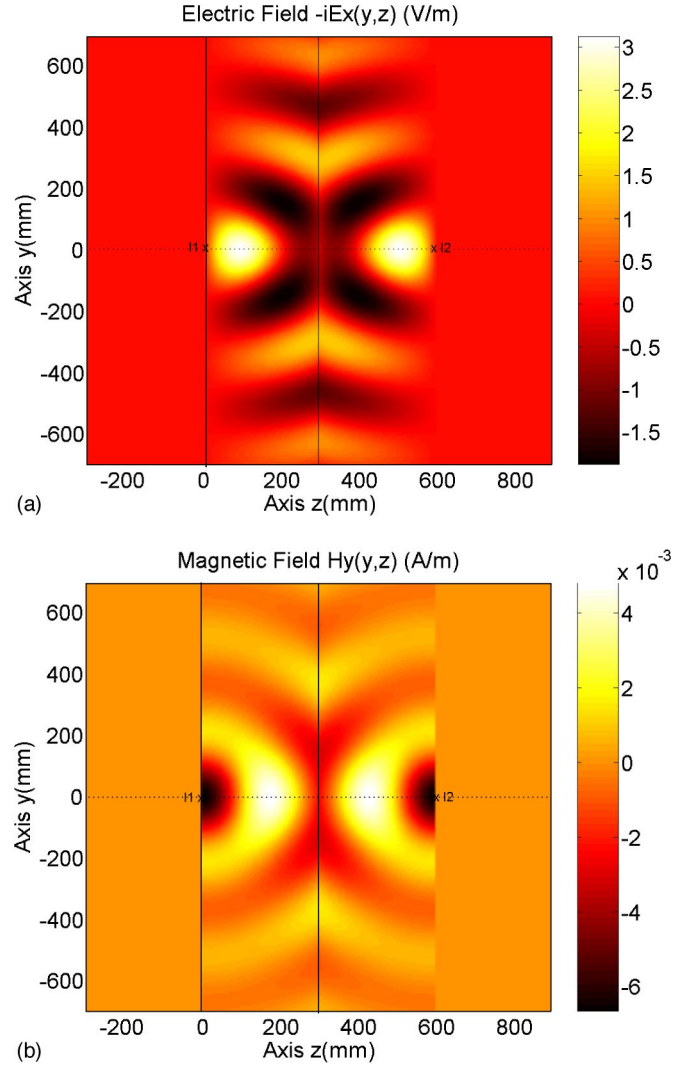


FIG. 4. (Color online) The field patterns of propagating waves within and outside the LHM slab when the frequency is 1 GHz and $d_1=0$ and $d_2=300$ mm. (a) Electric field E_{xp} . (b) Magnetic field H_{yp} .

$$T = \frac{4(1 + \delta)}{-\delta^2 + (2 + \delta)^2 e^{-2\gamma d}}. \quad (17)$$

Clearly, $T=e^{2\gamma d}$ for any evanescent spectra if $\delta=0$, which amplifies the evanescent waves to generate a perfect image at the perfect-imaging point $z=2d=2(d_2-d_1)$. If $\delta \neq 0$, however, the second item of the denominator approach 0 when $\gamma \rightarrow \infty$. Then the transmission coefficient T becomes a constant. It is obvious that evanescent waves cannot be amplified for large γ . This feature also makes the integrals in evanescent waves be integrable. In other words, the mismatch or loss prevents the lens from perfect imaging, as indicated in Refs. 26–29. Hence, the evanescent-wave parts corresponding to Eqs. (9), (14), and (15) have finite values, which represent strong surface waves.

First we consider a slight mismatch when $|\delta|=10^{-8}$. In order to observe the propagating and evanescent waves clearly, we have computed the electric and magnetic field distributions inside and outside the LHM slab when δ

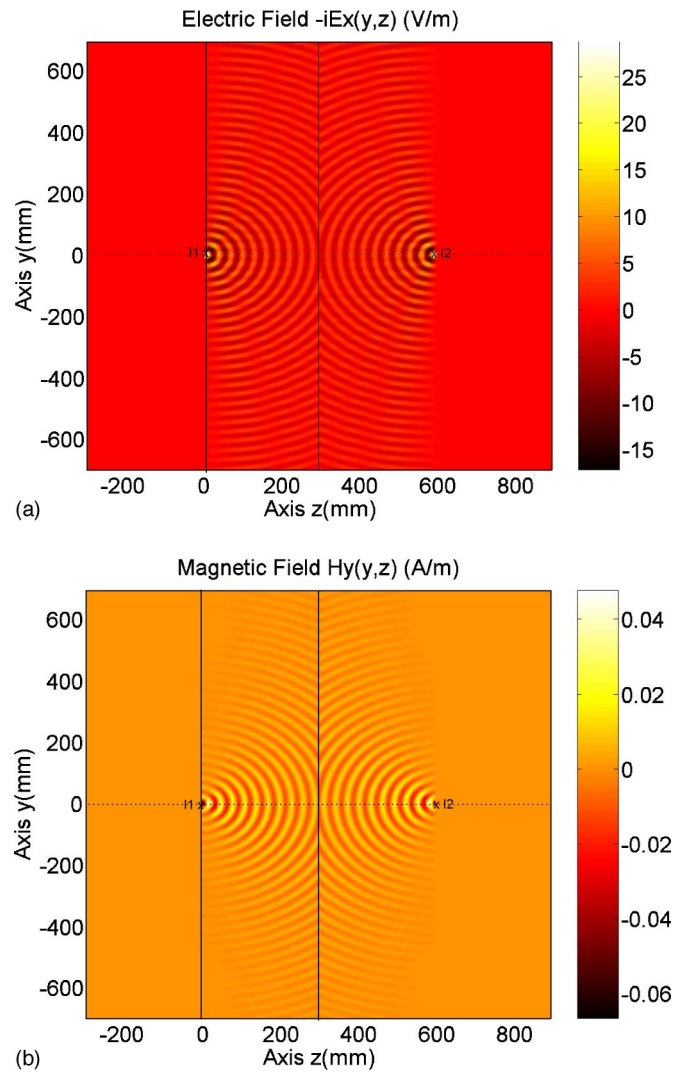
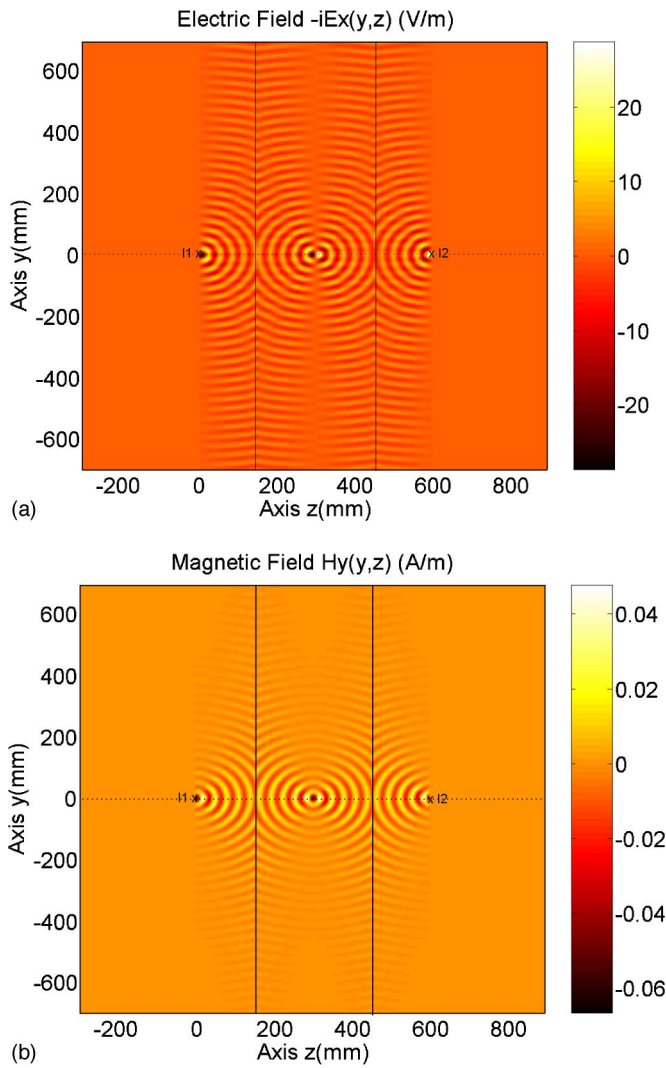


FIG. 5. (Color online) The field patterns of propagating waves within and outside the LHM slab when the frequency is 10 GHz and $d_1=150$ mm and $d_2=450$ mm. (a) Electric field E_{xp} . (b) Magnetic field H_{yp} .

FIG. 6. (Color online) The field patterns of propagating waves within and outside the LHM slab when the frequency is 10 GHz and $d_1=0$ and $d_2=300$ mm. (a) Electric field E_{xp} . (b) Magnetic field H_{yp} .

$=10^{-8}$, in which $d_1=150$ mm, $d_2=450$ mm, $I_1=1$ mA, $I_2=-1$ mA, and $f=1$ GHz. The propagating and evanescent parts of the fields are depicted separately for details, as shown in Figs. 7 and 8. Obviously, the thickness of the slab is 300 m, which is equal to the free-space wavelength. The computational domain is chosen as $-700 \leq y \leq 700$ and $-150 \leq z \leq 900$ (unit: mm) to include the source locations and the perfect-imaging points. Near the source locations, only field values at a small vicinity of 10^{-4} m around the sources are computed due to the singularity.

From Fig. 7, for the propagating waves, we clearly observe that the real part of electric field is much smaller than the imaginary part, and the imaginary part of magnetic field is much smaller than the real part. Comparing with the case of perfect lens shown in Fig. 2, the field distributions are nearly the same. Hence, the slight mismatch $\delta=10^{-8}$ has little effect on the propagating waves. All electromagnetic fields and energies are nearly confined in the region between the two sources.

For evanescent waves, the slight mismatch will result in strong surface waves along two boundaries of the slab, as shown in Fig. 8. From the simulations of single source located at origin, we notice that the slab boundaries are alternated with wave crests and wave troughs. Such wave crests and wave troughs can be either enhanced or cancelled when the other current source at the perfect-imaging point has an opposite direction. In the case of $\delta > 0$, the wave-crest (or wave-trough) positions of two sources are coincident together except in a small region close to the sources, which yields an enhancement of surface waves, as shown in Fig. 8. Clearly, the evanescent waves are highly concentrated near the boundaries of the slab, and they are also confined in the region between the two sources.

In the case of $\delta=-10^{-8}$, the propagating waves have similar behaviors to those of $\delta=10^{-8}$. In evanescent waves, however, the wave-crest/trough positions of one source are just the wave-trough/crest positions of another except in a small region close to the sources for both electric and magnetic

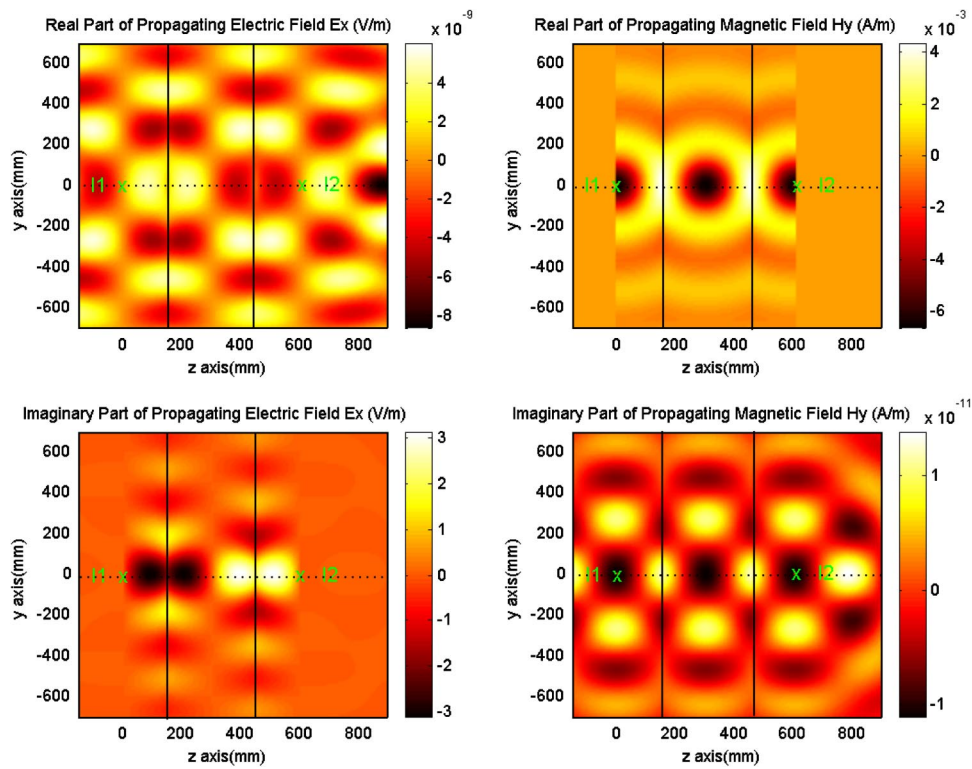


FIG. 7. (Color online) Field distributions of propagating waves excited by two current sources with opposite directions by a LHM slab, where $\delta=10^{-8}$, $d_1=150$ mm, $d_2=450$ mm, and $f=1$ GHz. The left figures are electric field and the right figures are magnetic field distributions, indicating the real and imaginary parts from the top to the bottom.

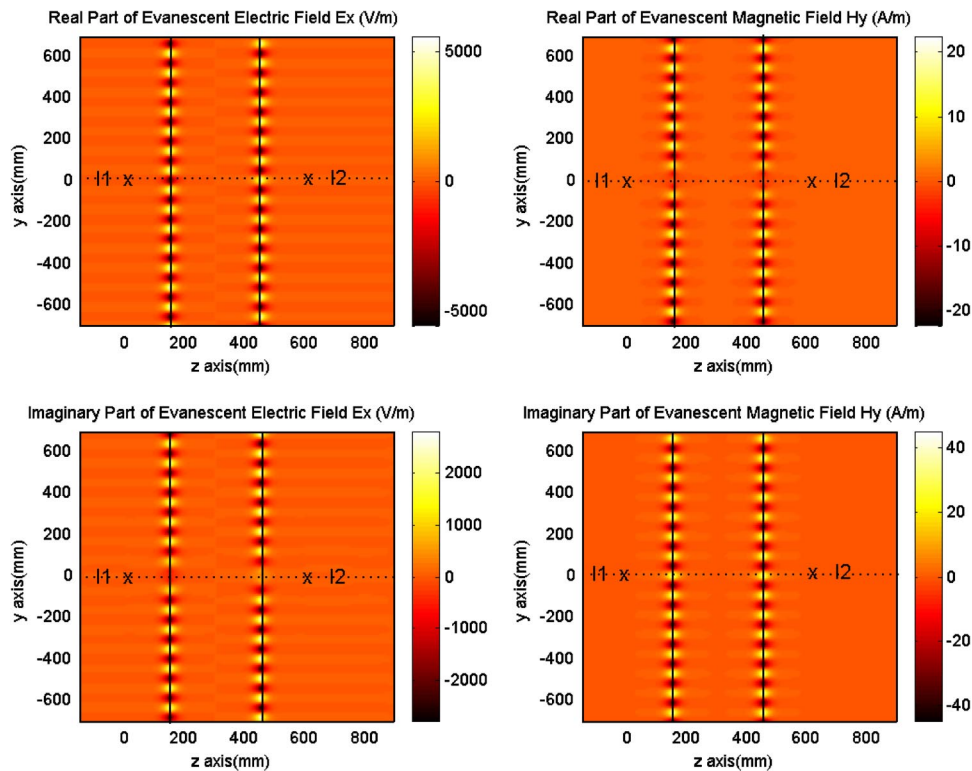


FIG. 8. (Color online) Field distributions of evanescent waves excited by two current sources with opposite directions by a LHM slab, where $\delta=10^{-8}$, $d_1=150$ mm, $d_2=450$ mm, and $f=1$ GHz. The left figures are electric field and the right figures are magnetic field distributions, indicating the real and imaginary parts from the top to the bottom.

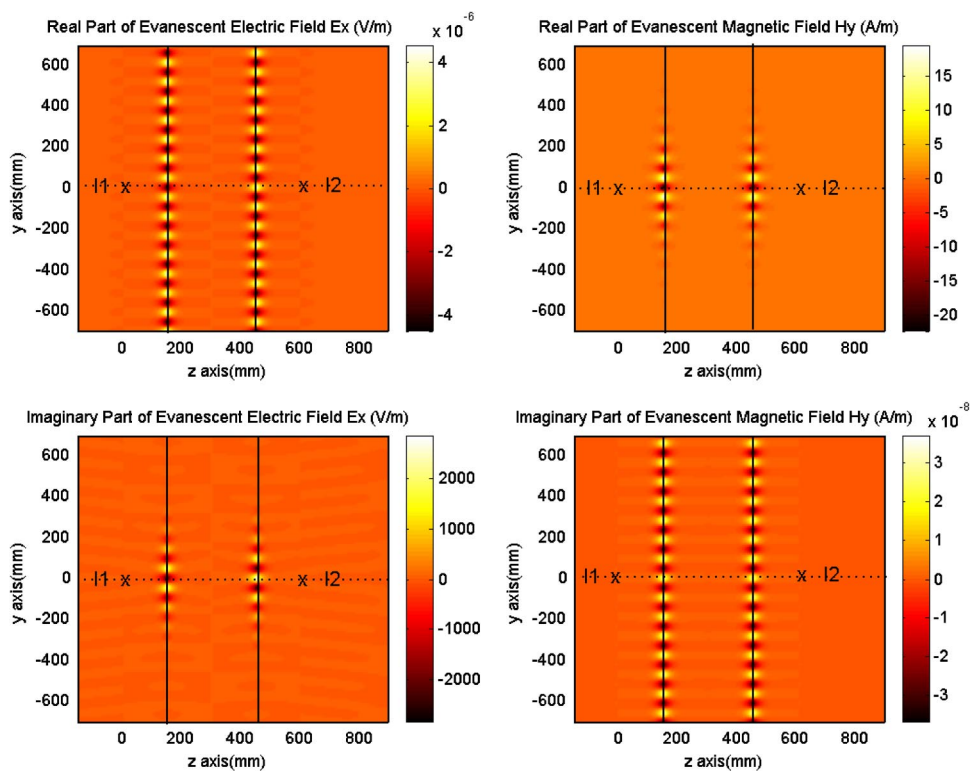


FIG. 9. (Color online) Field distributions of evanescent waves excited by two current sources with opposite directions by a LHM slab, where $\delta = -10^{-8}$, $d_1 = 150$ mm, $d_2 = 450$ mm, and $f = 1$ GHz. The left figures are electric field and the right figures are magnetic field distributions, indicating the real and imaginary parts from the top to the bottom.

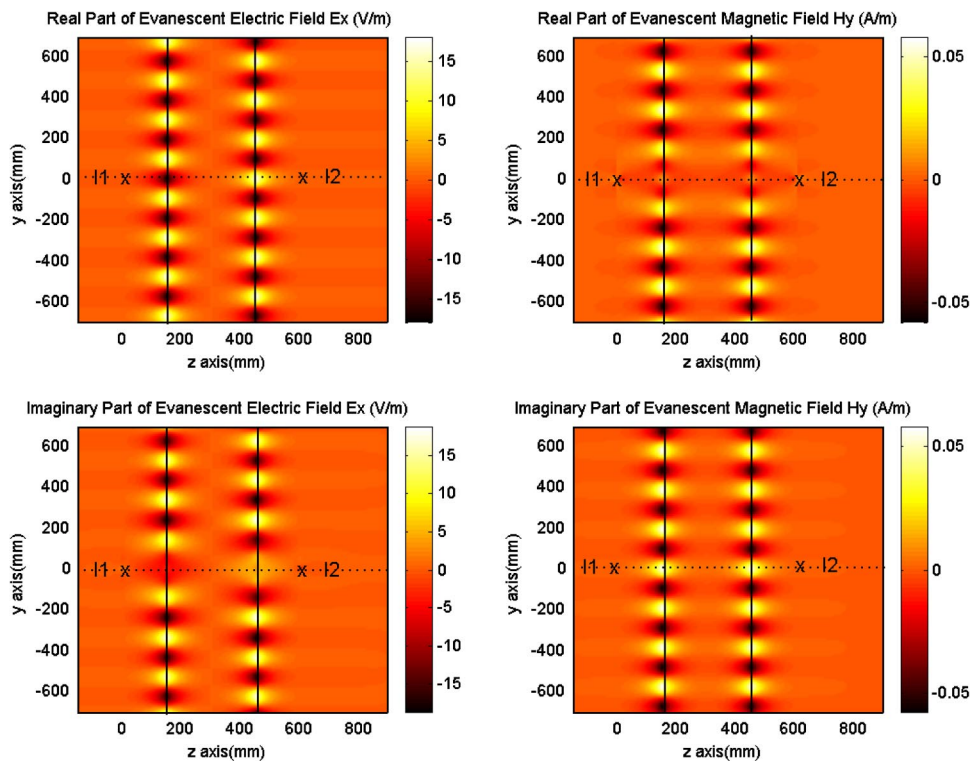


FIG. 10. (Color online) Field distributions of evanescent waves excited by two current sources with opposite directions by a LHM slab, where $\delta = 10^{-3}$, $d_1 = 150$ mm, $d_2 = 450$ mm, and $f = 1$ GHz. The left figures are electric field and the right figures are magnetic field distributions, indicating the real and imaginary parts from the top to the bottom.

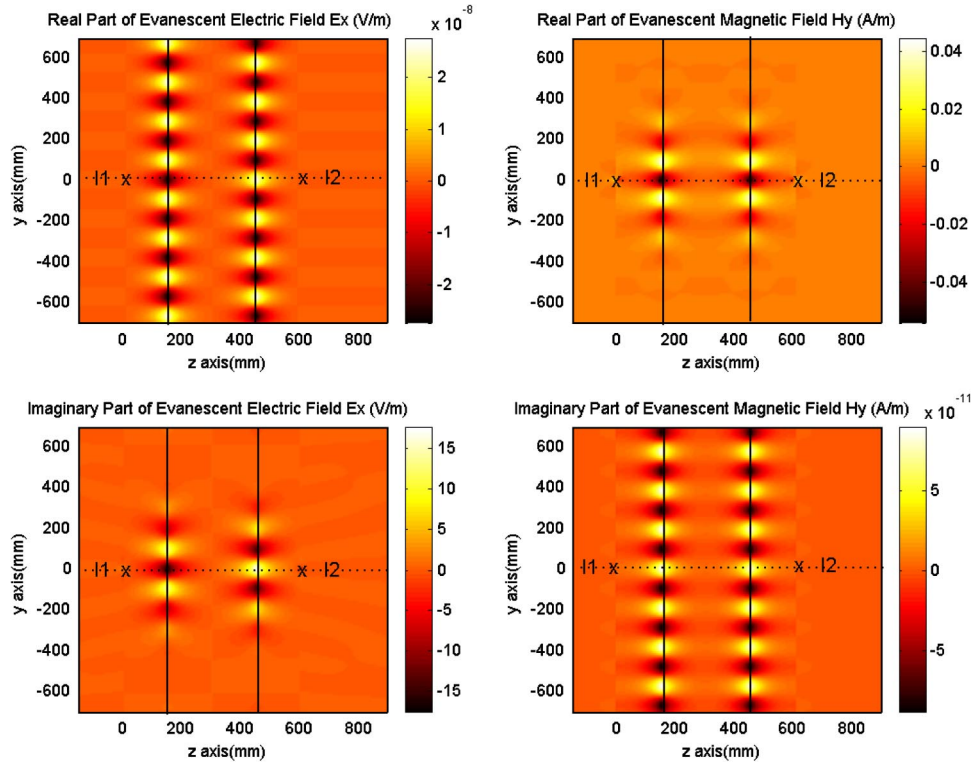


FIG. 11. (Color online) Field distributions of evanescent waves excited by two current sources with opposite directions by a LHM slab, where $\delta = -10^{-3}$, $d_1 = 150$ mm, $d_2 = 450$ mm, and $f = 1$ GHz. The left figures are electric field and the right figures are magnetic field distributions, indicating the real and imaginary parts from the top to the bottom.

fields. Hence, the surface waves far from the sources will be cancelled each other, and strong surface waves are only confined in small regions near the sources, as illustrated in Fig. 9. This is obviously a localization of electromagnetic waves. From Fig. 9, we also notice that the imaginary part of the electric field is much larger than its real part, and the real part of the magnetic field is much larger than its imaginary part. As a consequence, the Poynting vector $\mathbf{S} = \mathbf{E} \times \mathbf{H}^*$ has a much larger imaginary part than the real part. This means that the power radiation is much less than the exchange of electric and magnetic energies. Therefore, the energy is highly concentrated in the small region, which will be very useful in engineering such as the design of medical equipments.

When the LHM slab has a larger mismatch to the RHM background with $|\delta| = 10^{-3}$, the simulation results of electric and magnetic fields excited by two current sources located at the perfect-imaging points are shown in Figs. 10 and 11, in which Fig. 10 illustrates the case of positive δ , and Fig. 11 illustrates the case of negative δ . Here, only the evanescent waves are plotted because the propagating waves have similar behaviors to those of $\delta = 10^{-8}$. Comparing Figs. 10 and 11 with Figs. 8 and 9, we observe similar physical phenomena except the following two differences. (1) When $|\delta|$ is larger, the frequency of surface waves along slab edges becomes smaller. In other words, the wavelength of surface waves becomes longer, which is consistent with the analysis in Refs. 25–27. (2) When $|\delta|$ is larger, the evanescent waves are less concentrated around the two surfaces of the slab, in which the field values are much lower than those for $|\delta|$

$= 10^{-8}$. This is coincident with the earlier perfect-matching analysis, where the evanescent waves tend to infinity when $\delta = 0$.

As a comparison, we consider the radiation of the same current sources at the same positions by a RHM slab where $\mu_{r2} = 1 + \delta$ and $\epsilon_{r2} = 1/(1 + \delta)$. Figure 12 demonstrates the field distributions when $\delta = -10^{-3}$. We observe that the surface waves do not exist at all for RHM slab because the poles of integrands are located in the lower Riemann sheet in the k_z plane, and none of them is located on the integration path. Note that in Fig. 12 the real part of magnetic field is not very clear since the large values near the sources submerge other information of the field. But the localization of electromagnetic waves is not observed. In other words, only the LHM slab can localize electromagnetic waves.

Finally, we study the effect of different phase differences between two sources on the energy localization. Consider an extreme case when the two currents have the same directions, i.e., the in-phase case. Then the simulation results of electric and magnetic fields for propagating and evanescent waves are illustrated in Figs. 13 and 14, where $\delta = 10^{-3}$. From Fig. 13, we notice that the propagating waves cannot be confined in the region between the two source, and hence, the propagating energies cannot be localized. For evanescent waves, however, the strong surface waves are mainly confined in the small region although a small amount energies are radiated out, as shown in Fig. 14.

Figure 14 also demonstrates that the real part of electric field is much smaller than the imaginary part, and the imaginary part of magnetic field is much smaller than the real part.

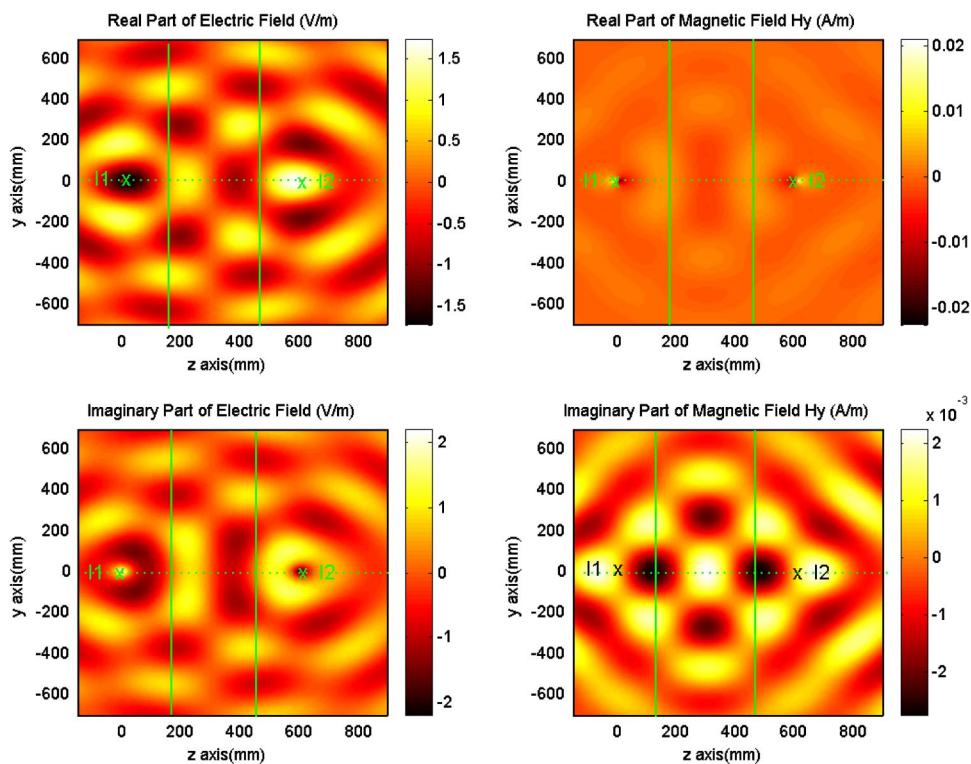


FIG. 12. (Color online) Field distributions excited by two current sources with opposite directions by a RHM slab, where $\delta = -10^{-3}$, $d_1 = 150$ mm, $d_2 = 450$ mm, and $f = 1$ GHz. The left figures are electric field and the right figures are magnetic field distributions, indicating the real and imaginary parts from the top to the bottom.

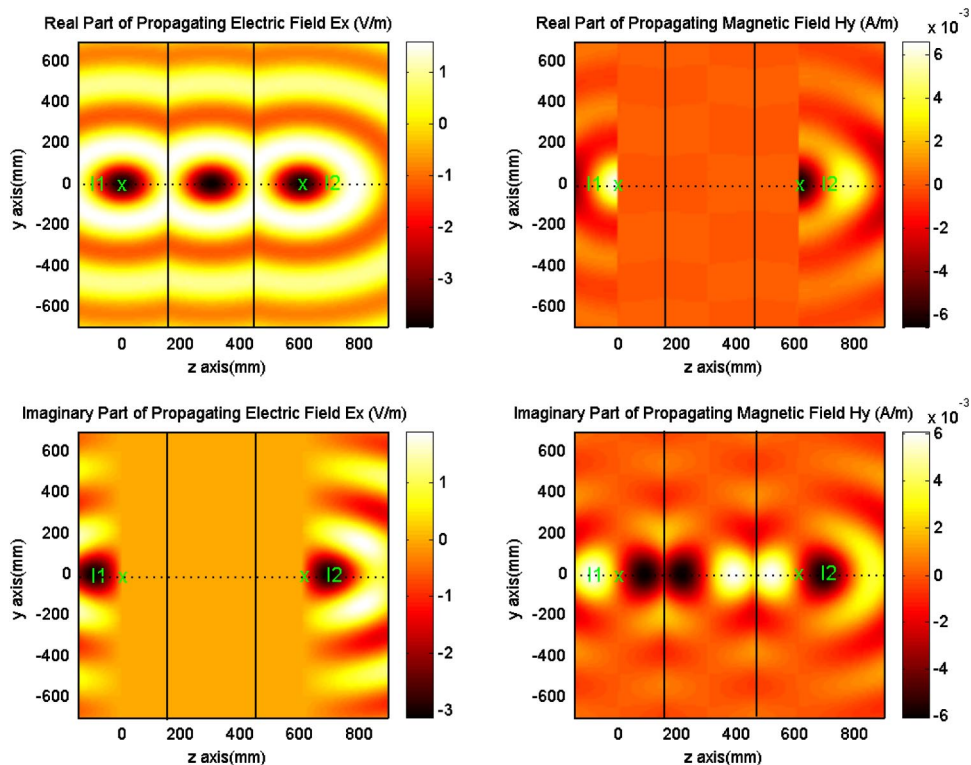


FIG. 13. (Color online) Field distributions of propagating waves excited by two current sources with the same directions by a LHM slab, where $\delta = 10^{-3}$, $d_1 = 150$ mm, $d_2 = 450$ mm, and $f = 1$ GHz. The left figures are electric field and the right figures are magnetic field distributions, indicating the real and imaginary parts from the top to the bottom.

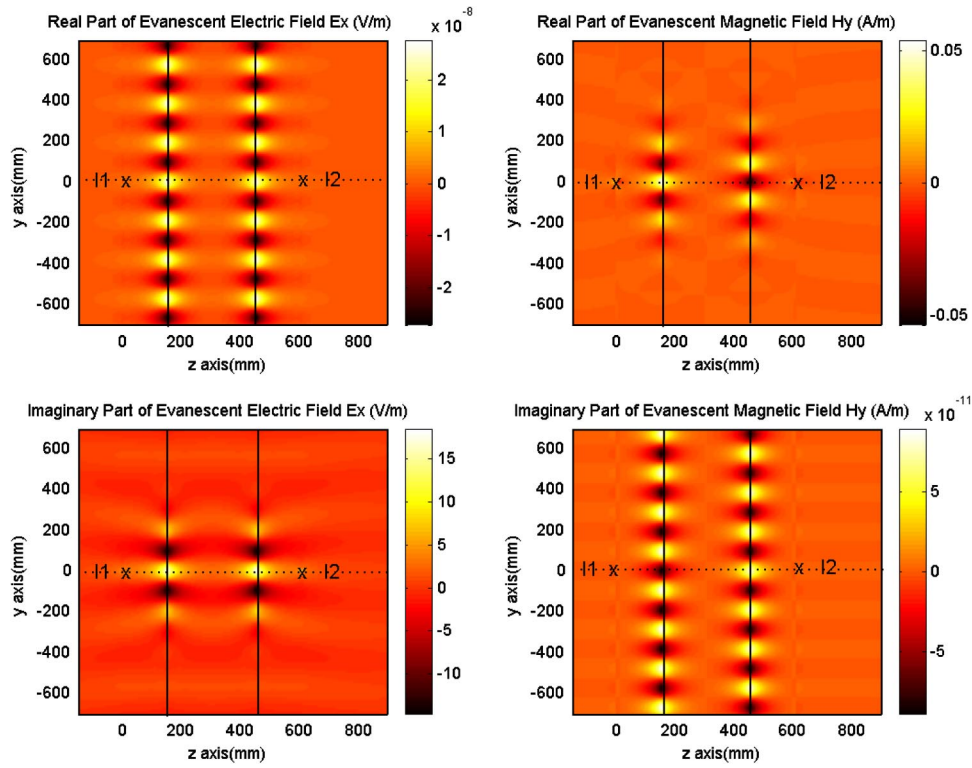


FIG. 14. (Color online) Field distributions of evanescent waves excited by two current sources with the same directions by a LHM slab, where $\delta=10^{-3}$, $d_1=150$ mm, $d_2=450$ mm, and $f=1$ GHz. The left figures are electric field and the right figures are magnetic field distributions, indicating the real and imaginary parts from the top to the bottom.

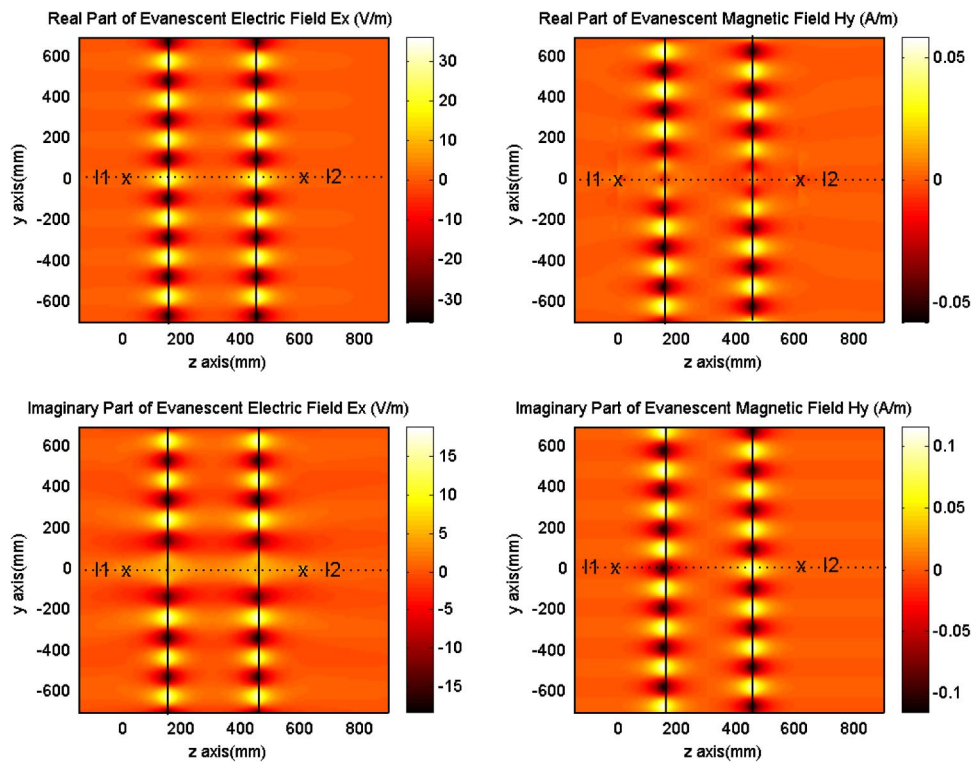


FIG. 15. (Color online) Field distributions of evanescent waves excited by two current sources with the same directions by a LHM slab, where $\delta=-10^{-3}$, $d_1=150$ mm, $d_2=450$ mm, and $f=1$ GHz. The left figures are electric field and the right figures are magnetic field distributions, indicating the real and imaginary parts from the top to the bottom.

It is interesting to see Fig. 14 is quite similar to Fig. 11. This is because similar cancellation happens in surface waves when the source currents have the same directions and $\delta > 0$ to the case when the currents have opposite directions and $\delta < 0$. Using the same principle, similar enhancement occurs in surface waves when the source currents have the same directions and $\delta < 0$ to the case when the currents have opposite directions and $\delta > 0$. The simulation results of evanescent waves are shown in Fig. 15. Although the electromagnetic energies are mainly confined in the region between two sources, there are notable energies radiated out.

IV. CONCLUSIONS

Through an exact analysis, we have shown that a lossless LHM slab with negative permittivity $-\epsilon_0$ and negative permeability $-\mu_0$ can highly localize the electromagnetic energy in a small region completely. When two linear sources with opposite current directions are placed at the perfect-imaging points of the LHM slab, all electromagnetic waves are confined in the region between the two sources and there is no power radiating outside and no power transmitting inside. The propagating modes of such electromagnetic waves behave like standing waves, and the evanescent modes behave

like plasma surface waves. The filed patterns inside the region can be controlled by changing the source positions.

When the LHM slab has a slight mismatch with the free-space background, i.e., $\mu_{r2} = -(1 + \delta)$ and $\epsilon_{r2} = -1/(1 + \delta)$, we have demonstrated that such a LHM slab can also localize electromagnetic waves, where both the propagating and evanescent parts of electromagnetic waves are nearly confined within the region between the two sources. If $\delta < 0$, the evanescent waves are even confined in a small region around the sources and inside the slab. Numerical experiments have verified the above conclusions. Such localizations of electromagnetic waves may find important applications in new microwave and optical devices.

ACKNOWLEDGMENTS

This work was supported in part by the National Science Foundation of China for Distinguished Young Scholars under Grant No. 60225001, in part by the National Science Foundation of China under Grant No. 60496317, in part by the National Basic Research Program (973) of China under Grant No. 2004CB719800, and in part by the National Doctoral Foundation of China under Grant No. 20040286010.

*Email address: tjcui@seu.edu.cn

- ¹V. G. Veselago, *Sov. Phys. Usp.* **10**, 509 (1968).
- ²J. B. Pendry, A. J. Holden, W. J. Stewart, and I. Youngs, *Phys. Rev. Lett.* **76**, 4773 (1996).
- ³J. B. Pendry, A. J. Holden, D. J. Robbins, and W. J. Stewart, *IEEE Trans. Microwave Theory Tech.* **47**, 2075 (1999).
- ⁴R. A. Shelby, D. R. Smith, S. C. Nemat-Nasser, and S. Schultz, *Appl. Phys. Lett.* **78**, 489 (2000).
- ⁵D. R. Smith, W. J. Padilla, D. C. Vier, S. C. Nemat-Nasser, and S. Schultz, *Phys. Rev. Lett.* **84**, 4184 (2000).
- ⁶R. A. Shelby, D. R. Smith and S. Schultz, *Science* **292**, 77 (2001).
- ⁷D. R. Smith and N. Kroll, *Phys. Rev. Lett.* **85**, 2933 (2000).
- ⁸R. W. Ziolkowski, *Phys. Rev. E* **63**, 046604 (2001).
- ⁹P. M. Valanju, R. M. Walser, and A. P. Valanju, *Phys. Rev. Lett.* **88**, 187401 (2002).
- ¹⁰J. Pacheco, Jr., T. M. Grzegorzcyk, B. I. Wu, Y. Zhang, and J. A. Kong, *Phys. Rev. Lett.* **89**, 257401 (2002).
- ¹¹N. Garcia and M. Nieto-Vesperinas, *Phys. Rev. Lett.* **88**, 207403 (2002).
- ¹²M. W. Feise, P. J. Bevelacqua, and J. B. Schneider, *Phys. Rev. B* **66**, 035113 (2002).
- ¹³D. R. Smith, D. Schurig, M. Rosenbluth, S. Schultz, S. A. Ramakrishna, and J. B. Pendry, *Appl. Phys. Lett.* **82**, 1506 (2003).
- ¹⁴R. W. Ziolkowski and N. Engheta, *IEEE Trans. Antennas Propag.* **10**, 2546 (2003).
- ¹⁵J. B. Pendry, *Phys. Rev. Lett.* **85**, 3966 (2000).
- ¹⁶J. A. Kong, B. I. Wu, and Y. Zhang, *Appl. Phys. Lett.* **80**, 2084 (2002).
- ¹⁷S. A. Ramakrishna and J. B. Pendry, *J. Mod. Opt.* **49**, 1747 (2002).
- ¹⁸M. Bayindir *et al.*, *Appl. Phys. Lett.* **81**, 120 (2002).
- ¹⁹L. Wu, S. He, and L. Shen, *Phys. Rev. B* **67**, 235103 (2003).
- ²⁰N. C. Panoiu and R. M. Osgood, *Phys. Rev. E* **68**, 016611 (2003).
- ²¹T. J. Cui, Z. C. Hao, X. X. Yin, W. Hong, and J. A. Kong, *Phys. Lett. A* **323**, 484 (2004).
- ²²S. John, *Phys. Rev. Lett.* **58**, 2486 (1997).
- ²³M. W. Takeda, S. Kiriwara, Y. Miyamoto, K. Sakoda, and K. Honda, *Phys. Rev. Lett.* **92**, 093902 (2004).
- ²⁴K. Sakoda, *Optical Properties of Photonic Crystals* (Springer-Verlag, Berlin, 2001).
- ²⁵J. Lu, T. M. Grzegorzcyk, B.-I. Wu, J. Pacheco, M. Chen, and J. A. Kong, *Microwave Opt. Technol. Lett.* (to be published).
- ²⁶D. R. Smith, D. Schurig, M. Rosenbluth, S. Schultz, S. A. Ramakrishna, and J. B. Pendry, *Appl. Phys. Lett.* **82**, 1506 (2003).
- ²⁷N. Zhang and X. Zhang, *Appl. Phys. Lett.* **82**, 161 (2003).
- ²⁸R. Merlin, *Appl. Phys. Lett.* **84**, 1290 (2004).
- ²⁹L. Chen, S. He, and L. Shen, *Phys. Rev. Lett.* **92**, 107404 (2004).